Mon. Not. R. Astron. Soc. **000**, 1–4 (2008) Printed 9 December 2009 (MN LATEX style file v2.2)

Correlations between gas, star and dark matter components of halos in a SPH simulation

Pascal S. P. Steger[1], Oliver J. Hahn[1], ⋆, C. Marcella Carollo[1], Cristiano Porciani[1] and Giuseppe Tormen[2]
[1]*Department of Physics, ETH Zürich, CH-8093 Zürich, Switzerland*
[2]*Dipartimento di Astronomia, Università di Padova, Vicolo dell'Osservatorio 2, I-35122 Padova, Italy*

Draft Version 9 December 2009

ABSTRACT

simulate mergers, looking at dm halo (mass loss, final angular momentum, conservation of momentum)
dynamical process: heating of gas, quantitative, as fct of...
picture of galaxy =¿ dm halo mass, angular momentum, density distribution
correction of images for weak lensing: get distribution of dm
distribution of dark energy throughout universe: uniform/follows nrj/concentrated in voids?
galaxies as spinning tops: precession of stars/gas/dm shells as fct of environment/mass/form/angular momentum
detection of cosmic neutrino background/predictions
influence of finite c on information propagation for large structures/in the early universe
influence of dm gravitational field on spectra of stars/galaxies?
fractal properties of mass distribution as fct of scale

Key words: cosmology: theory, large-scale structure of Universe – galaxies: formation, evolution – methods: numerical

1 INTRODUCTION

The article is organized as follows: Chapter 2 gives an overview over the specifics of the simulations used, definitions are given in chapter 3. Chapter 4 then includes two checks for the plausibility of simulations and our pipeline and our findings for the disalignment between angular momentum, main inertia axis and tidal field eigenvectors. We conclude the article with a discussion in chapter 5.

2 THE DATA

2.1 Specifics of the Simulations

We use high-resolution cosmological hydrodynamic simulations of three individual galaxy clusters embedded in a cosmological box of $192\,h^{-1}\mathrm{Mpc}$. The cosmological model assumes a flat Λ-CDM cosmology with matter density parameter $\Omega_m = 0.3$, baryon fraction $\Omega_b = 0.04$, Hubble constant $H_0 = 70\,\mathrm{km\,s^{-1}\,Mpc^{-1}}$ and a power spectrum normalization of $\sigma_8 = 0.8$. The simulations were performed using the tree-SPH+N-body code GADGET-2 (Springel 2005) and include subgrid models for cooling, star formation and stellar feedback identical to the simulations described by Borgani et al. (2004). The three galaxy clusters were resimulated at 45 times higher resolution giving a mass resolution of $1.03 \times 10^7\,h^{-1}\mathrm{M}_\odot$ for the dark matter component, while gas and stars were both sampled with particles of mass $7.7 \times 10^6\,h^{-1}\mathrm{M}_\odot$. Dark matter particles in the outskirt of the simulation box have varying masses above $5.33 \times 10^9\,h^{-1}\mathrm{M}_\odot$. The simulations were started at $z = 100$ and evolved until $z = 0$ where we perform our analysis. The properties of the three resimulated clusters at $z = 0$ are summarized in table 1.

Simulation	$M_{\rm vir}/h^{-1}\mathrm{M}_\odot$	$R_{\rm vir}/h^{-1}\mathrm{Mpc}$	$N_{\rm sub}$	$N_{\rm field}$
c1	2.8900×10^{14}	1.3466	502	218
c2	1.6021×10^{14}	1.1062	279	200
c3	2.4922×10^{14}	1.2817	399	163

Table 1. Properties of the resimulated clusters. $M_{\rm vir}$ and $R_{\rm vir}$ are the virial mass and radius of the clusters. The number of subhaloes above $M = 5 \cdot 10^9 h^{-1}\mathrm{M}_\odot$ within the cluster virial radius is given by $N_{\rm sub}$, while $N_{\rm field}$ is the number of isolated haloes above $M = 5 \cdot 10^9 h^{-1}\mathrm{M}_\odot$ within 3 virial radii from the cluster center.

⋆ E-mail: psteger@phys.ethz.ch, hahn@phys.ethz.ch

2.2 Halo and Subhalo Samples

Haloes and subhaloes in the high-resolution region were identified with the AMIGA halo finder (Knollmann et al., in preparation and Gill et al. (2004)) that identifies a hierarchy of gravitationally bound density peaks. Particles that are not gravitationally bound due to their streaming velocity and/or internal energy were removed in two steps. For each halo we determine the shape and angular momentum of gas, stars and dark matter as described below. For our analysis, we put together the haloes of all three clusters and constrain ourselves to haloes that have more than 200 dark matter, more than 50 gas and more than 100 star particles inside. Moreover, we exclude all haloes that contain low resolution dark matter particles with a mass bigger than 1% of the halo mass. If not specified otherwise, the figures were created using particles of all types together.

3 DEFINITIONS

3.1 Shapes

The shape of a halo with N particles is determined by its moment of inertia tensor

$$I_{jk} \equiv \sum_{i=1}^{N} m_i (r_i^2 \delta_{jk} - (x_i)_j (x_i)_k) \tag{1}$$

with the distance $r_i \equiv ((x_i)_1, (x_i)_2, (x_i)_3)$ of a particle at position x_i from the host center. Written in an eigensystem with eigenvectors $\mathbf{e}_1, \mathbf{e}_2, \mathbf{e}_3$, it reads as

$$\tilde{I} = \frac{M}{5} \cdot \mathrm{diag}(\ell_1^2 + \ell_3^2, \ell_1^2 + \ell_3^2, \ell_1^2 + \ell_2^2) \tag{2}$$

with the lengths of the pricipal axes $\ell_1 \geqslant \ell_2 \geqslant \ell_3$.

3.2 Angular Momentum

The classical definition of

$$\mathbf{J} = \sum_{i=1}^{N} \mathbf{r}_i \times m_i \mathbf{v}_i \tag{3}$$

is used to calculate the angular momentum in the center of mass frame. AMIGA used a slightly different method with concentric shells.

3.3 Halo Spin Parameter

Following Bullock et al. (2001), we define the spin parameter

$$\lambda' \equiv \frac{|\mathbf{J}|}{\sqrt{2} M R v} \tag{4}$$

with the angular momentum $\mathbf{J}$ inside a sphere of radius R, mass M and circular velocity v. As established by many previous studies, λ'_{DM} is best described by a log-normal distribution,

$$p(\lambda) d\lambda = \frac{1}{\sqrt{2\pi}\sigma_\lambda} \exp\left[-\frac{\ln^2(\lambda/\bar{\lambda})}{2\sigma_\lambda^2}\right] \frac{d\lambda}{\lambda}, \tag{5}$$

which is a simple parabola in a logarithmic plot.

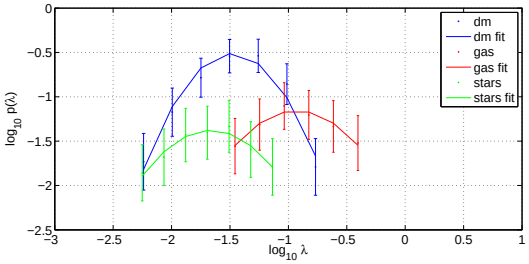

Figure 1. Halo spin parameter distribution for host haloes, with fitted parabolas. Dark matter produces the blue line, stars the green one, gas is shown in red. Stars follow dark matter and peak at around -1.5, while gas shows more ordered motion. See 2 for fitting parameters.

Halo Type	a	b	c
Dark Matter	-2.3 ± 0.7	-6.7 ± 2.0	-5.5 ± 1.4
Gas	-1.4 ± 0.6	-2.6 ± 1.1	-2.4 ± 0.5
Stars	-1.5 ± 0.5	-5.0 ± 1.8	-5.5 ± 1.5

Table 2. Fit parameters for λ'-distribution with errors for 95% level certainty.

3.4 Tidal Field

We compute the local eigenstructure of the smoothed tidal field tensor for each halo in order to probe the alignment with the large-scale structure (cf. Hahn et al. 2007). First, we solve Poisson's equation by Fast Fourier Transform on a grid of 512^3 cells for the smoothed overdensity field δ by the double convolution $\phi_R = \delta \star W_R \star G$, where G is the Green's function of the symmetric 3-point finite difference operator and W_R is the window function of scale R used to smooth the density field. The tidal tensor

$$T_{ij}(\mathbf{x}) \equiv \left[\partial_i \partial_j - \frac{1}{3}\delta_{ij}\nabla^2\right] \phi(\mathbf{x}) \tag{6}$$

is then evaluated at the positions of the halo centers by finite differencing. We finally compute eigenvalues $\tau_1 \geqslant \tau_2 \geqslant \tau_3$ and corresponding eigenvectors $\mathbf{t}_1, \mathbf{t}_2, \mathbf{t}_3$ for each halo.

4 RESULTS

4.1 Check I: Halo parameter distribution

Fig. 1 shows the λ' distribution for dark matter, gas and stars. Additional tails at high values of λ' were removed by centering on the most bound particle instead of the center of mass. With this procedure the ordered motion due to a close encounter with another halo is suppressed, cf. Hahn et al. (2007). λ' shows a log-normal distribution for dark matter, gas and stars; the maxima lie at -1.5 for dark matter and stars and at -1 for gas, respectively. If a parabola $y = ax^2 + bx + c$ is fitted through these points, one gets the parameters listed in table 2. The gas particles show a higher maximum for λ' and therefore more ordered motion compared to random motion. This is expected as the kinetic energy is transformed into heat which in turn escapes through radiation. The distribution for stars peaks at roughly the same place as the one for dark matter, which is what was found by Croft et al. (2008).

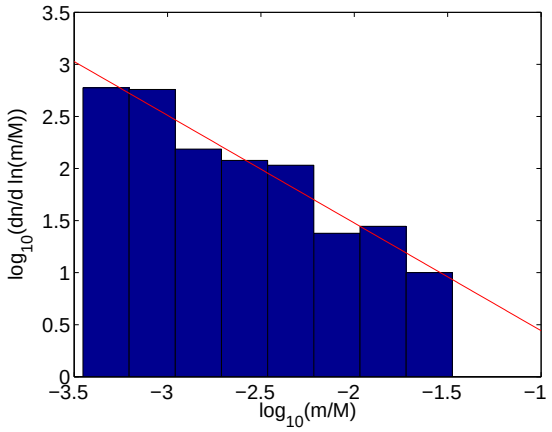

Figure 2. Subhalo mass function using the respective host halo with mass M, incorporating all particle types. All subhaloes with mass m such that $log_{10}(m/M) < -3.5$ are excluded since below this threshold the discreteness of the halo constituents and their different mass compositions imply that too little subhaloes of a given mass are counted.

4.2 Check II: Subhalo Mass Function

The subhalo mass function as shown in fig. 2 is in good agreement with the expected power law with a slope of -1.

4.3 Shapes

Figure 3 presents the radial alignment of the main inertia axis of the dark matter component with the radial vector as function of distance, as investigated by Pereira et al. (2008). We recover the expected behavior for the low mass range ($m < 10^{11}\mathrm{M}_{\odot}$), and find an even stronger correlation with a maximum around $r \gtrsim r_{\mathrm{vir}}$ for the high mass range; at radii higher than $1.5r_{\mathrm{vir}}$ statements are not possible anymore due to lack of statistics. The second and third row show the analog for gas and stellar components of the haloes. The star component was found to have a distance dependence that resembles the one for dark matter particles in the high mass regime, while it does not do so in the low mass regime. This could be explained by the fact that stars start to behave like dark matter particles once they are created and rearrange themselves in the potential mainly given by the dark matter. The correlation of the inertial axis for gas with the radial vector shows no distinct distance dependence.

4.4 Angular Momentum

We find that the angular momenta of the dark matter haloes and the gas constituents do well correlate with each other. The angular momentum disalignment is shown in fig. 4, split into host, field and primary subhaloes. We find that the correlation deviates from the previously noted distributionCroft et al. (2008) for host haloes, small angles between gas and dark matter haloes seem to be preferred. This effect does not show up if we divide all haloes into mass bins.

4.5 Tidal Field

We were able to reproduce the expected correlation between different components of the tidal field eigenvectors and the inertia axes,

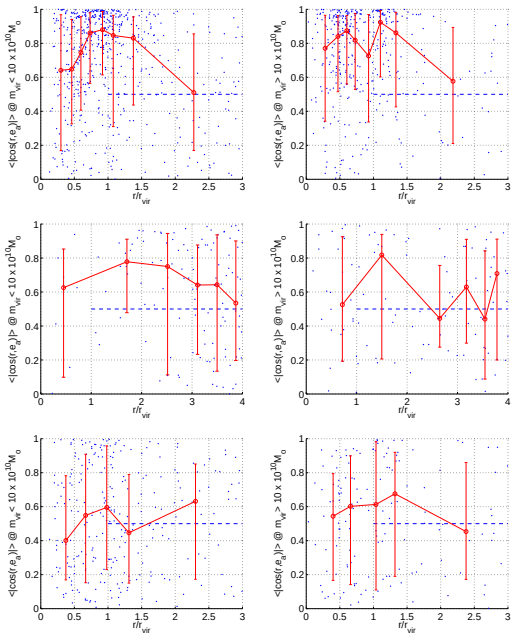

Figure 3. Distance dependence for the alignment between the main inertia axis $\mathbf{e}_1$ and the radial vector $\mathbf{r}$ to the cluster center. Panels on the left side include all haloes with mass $m < 10^{11}\mathrm{M}_{\odot}$, panels on the right side take all haloes into account with $m > 10^{11}\mathrm{M}_{\odot}$. Dark matter, gas and stellar components are shown in the first, second and third row.

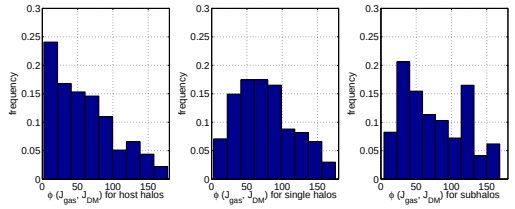

Figure 4. Distribution of angle ϕ between the angular momentum axis of dark matter and gas. The three bins contain host haloes (left), field haloes (middle) and primary subhaloes (right).

cf. Porciani et al. (2002), and found a similar correlation between tidal field and angular momentum, see fig. 5 and 6. TBD: cf. Porciani2002, TTT

5 SUMMARY AND DISCUSSION

TBD

ACKNOWLEDGMENTS

TBD. This work makes use of the NASA Astrophysics Data System.

6 APPENDIX: CHECKS

Both AMIGA and our HALOPROPERTIES were used to calculate the key features. When compared to each other with respect to

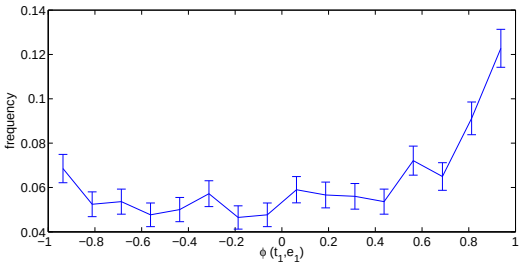

Figure 5. Correlation between $\mathbf{t}_1$, tidal field eigenvector corresponding to biggest eigenvalue of T_{ij}, and main inertia axis $\mathbf{e}_1$. The smoothing scale for the tidal field is $1\,h^{-1}\mathrm{Mpc}$.

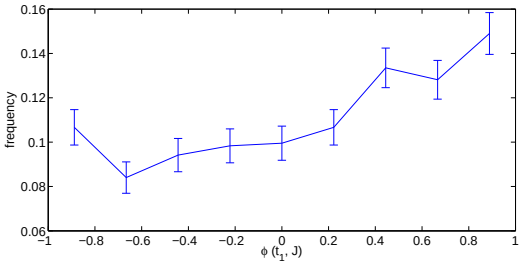

Figure 6. Correlation between $\mathbf{t}_1$ and angular momentum $\mathbf{J}$ for a smoothing scale of $1\,h^{-1}\mathrm{Mpc}$

angular momentum (where AMIGA uses concentric shells), they show a very close agreement for the vast majority of the haloes. The virial masses show a linear dependence – HALOPROPERTIES overestimates some of the values due to the fact that it does not use a spherical overdensity criterion, but does also include particles from outside r_{200}.

REFERENCES

Borgani S., Murante G., Springel V., Diaferio A., Dolag K., Moscardini L., Tormen G., Tornatore L., Tozzi P., 2004, MNRAS, 348, 1078
Bullock J. S., Dekel A., Kolatt T. S., Kravtsov A. V., Klypin A. A., Porciani C., Primack J. R., 2001, ApJ, 555, 240
Croft R. A. C., Di Matteo T., Springel V., Hernquist L., 2008, ArXiv e-prints
Gill S. P. D., Knebe A., Gibson B. K., 2004, MNRAS, 351, 399
Hahn O., Carollo C. M., Porciani C., Dekel A., 2007, MNRAS, 381, 41
Hahn O., Porciani C., Carollo C. M., Dekel A., 2007, MNRAS, 375, 489
Pereira M. J., Bryan G. L., Gill S. P. D., 2008, ApJ, 672, 825
Porciani C., Dekel A., Hoffman Y., 2002, MNRAS, 332, 339
Springel V., 2005, MNRAS, 364, 1105